A Wideband Dual-Polarized Endfire Antenna Array With Overlapped Apertures and Small Clearance for 5G Millimeter-Wave Applications

Hao Li, Yue Li, *Senior Member, IEEE*, Le Chang, Wangyu Sun, *Graduate Student Member, IEEE*, Xu Qin, and Hanyang Wang, *Senior Member, IEEE*

***Abstract*— In this article, an endfire dual-polarized phased antenna array with small ground clearance is proposed for the fifth-generation (5G) millimeter-wave (mmW) applications with a wide bandwidth. In this array, each antenna element consists of a dipole fed by a microstrip line for horizontal polarization and an H-plane horn using substrate-integrated waveguide (SIW) for vertical polarization. To achieve a wide bandwidth for vertical polarization, two metal vias are added at the aperture of the horn antenna. Then, a four-element antenna array is designed by partially overlapping the aperture of each horn element. A prototype has been fabricated using multilayer printed circuit board (PCB) process. The measured results agree well with the simulated ones. The antenna is with an impedance bandwidth of $|S_{11}| < -10$ dB from 24.4 to 29.5 GHz for both polarizations. The maximum gains of vertical and horizontal polarizations are 9.16 and 9.27 dBi, with the scanning angle from −34° to 33° for both polarizations with gain deterioration less than 3 dB. The proposed antenna is a promising solution for 5G mmW cellphones or antenna-in-package applications.**

***Index Terms*— Antenna array, antenna diversity, broadband antennas, millimeter-wave (mmW) antennas, mobile antennas.**

I. Introduction

DRIVEN by the rapid growth of the fifth-generation (5G) communication, the millimeter-wave (mmW) techniques have drawn significant researching interests [1]–[4]. In this band, the wide spectrum provides feasible opportunities to achieve high channel capacity. Researches have been widely launched on mmW antennas for different applications [5]–[9]. Considering high path loss of electromagnetic waves propagating at mmW bands [10], dual-polarized (DP) or polarization-reconfigurable antenna arrays are adopted to achieve high gains for arbitrary polarizations. Numerous works have been completed on DP or polarization-reconfigurable mmW antenna arrays for broadside radiation patterns [11]–[17]. In [14], a DP magnetoelectric dipole array has been proposed with wideband performance. Using the low-temperature cofire ceramics (LTCC) technology, a DP cavity antenna has been proposed for the mmW antenna in package (AiP) systems [15]. Other antennas including Fabry–Perot antennas [16] and dielectric resonator antennas [17] are also adopted in mmW bands. Meanwhile, antennas designed for 5G wireless communication have been investigated [18].

To achieve a full-space beam coverage, antennas with endfire radiation patterns are also required. Dipole arrays are usually used to generate horizontal polarized (H-pol) radiations with simple structure and compact size [19]–[21]. For the vertical polarized (V-pol) ones, the substrate-integrated waveguide (SIW) horn antenna is the first choice but usually suffers from narrow band in such low profile. By loading gradient dielectrics [22], [23], transition plates [24]–[26], or periodical structures [27], the impedance bandwidth can be improved at the expense of large clearance. Furthermore, other approaches have been adapted to realize DP endfire antenna arrays [28]–[32]. In [30] and [31], the slope-shaped slots are adopted as polarizers to generate an H-pol mode. These dielectrics are loaded in front of the apertures for impedance matching but increasing the clearance. Therefore, it is still a challenge to realize a DP endfire antenna array within small clearance and low profile.

In this article, as shown in Fig. 1, a DP four-element antenna array is proposed for mmW frequencies by combining SIW horns and dipoles. The proposed antenna array is placed on a complete ground plane for the requirements of handsets or AiP applications. The V-pol bandwidth is enhanced by loading vias on the horn apertures without extra ground clearance occupied. To further reduce the distance, the elements are arranged with part of apertures overlapping with adjacent ones. A prototype has been fabricated and measured. Within a thickness of 2.2 mm and a small clearance of 1.8 mm, the proposed antenna covers a wide bandwidth from 24.4 to 29.5 GHz in which the reflection coefficients are lower than −10 dB. Meanwhile, the antenna array performs a high gain of 9.16 dBi and a 3 dB beam steering range from −34° to 33°. The proposed antenna array is with merits of wide bandwidth,

Manuscript received April 1, 2020; revised June 15, 2020; accepted July 6, 2020. Date of publication August 19, 2020; date of current version February 3, 2021. This work was supported in part by Huawei Technologies, in part by the Natural Science Foundation of Beijing Manipulate under Contract 4182029, in part by the Tsinghua University Initiative Scientific Research Program under Contract 2019Z08QCX16, and in part by the Youth Top Program of Beijing Outstanding Talent Funding Project. *(Corresponding author: Yue Li.)*

Hao Li, Yue Li, Wangyu Sun, and Xu Qin are with the Department of Electronic Engineering, Tsinghua University, Beijing 100084, China, and also with the Beijing National Research Center for Information Science and Technology, Tsinghua University, Beijing 100084, China (e-mail: lyee@tsinghua.edu.cn).

Le Chang is with the Consumer Business Group of Huawei Inc., Beijing 100095, China (e-mail: changle5@huawei.com).

Hanyang Wang is with the Consumer Business Group of Huawei Inc., Reading RG2 6UF, U.K. (e-mail: hanyang.wang@huawei.com).

Color versions of one or more of the figures in this article are available online at https://ieeexplore.ieee.org.

Digital Object Identifier 10.1109/TAP.2020.3016512

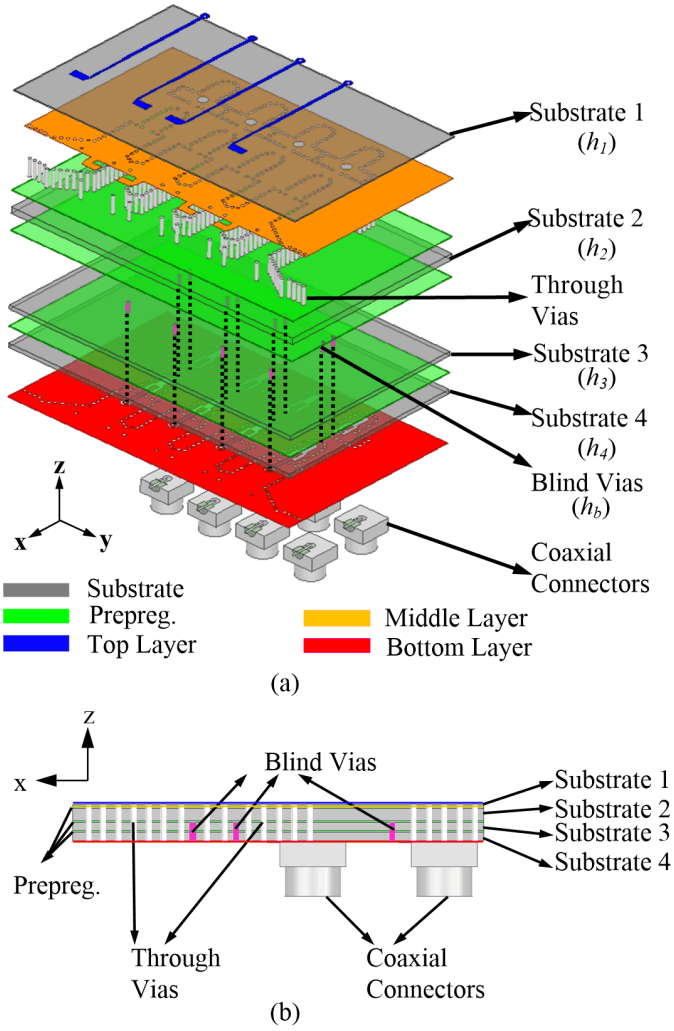

Fig. 1. Configuration of the proposed antenna array from (a) exploded view and (b) side view.

wide beam steering range, and small ground clearance for mmW applications.

II. Antenna Configuration and Operating Principle

A. Antenna Array Configuration

As plotted in Fig. 1(a), the proposed antenna array is constructed on a multilayer printed circuit board (PCB) with four substrate layers (Substrates 1–4), three prepreg layers, and three metal layers (top layer, middle layer, and bottom layer). The substrate (gray) is Taconic TLY-5 with a relative permittivity of 2.2 and a loss tangent of 0.0009. The prepreg (green) is Taconic FR-28 with a relative permittivity of 2.8 and a loss tangent of 0.004. The side view of all the substrate layers and vias is shown in Fig. 1(b). The through vias are drilled from Substrate 1 to Substrate 4. To see the detail on the middle layer and bottom layer, the through vias in Substrate 1 and Substrate 4 are not shown in Fig. 1(a). All through vias are connected to the middle layer except four feeding vias of the dipoles on the top layer. The four vias are connected with the microstrip lines on the top layer through the four holes on

TABLE I
Detailed Dimensions

Parameter	Value (mm)	Parameter	Value (mm)	Parameter	Value (mm)
h_1	0.508	h_2	0.508	h_3	0.762
h_4	0.127	h_p	0.1	h_b	1.116
l_1	2.8	l_2	5.6	l_3	2.1
l_4	4	l_5	12.8	l_6	4.4
l_d	4	l_f	2.5	w_1	4.6
w_2	6.8	w_3	4.8	w_4	33.4
w_5	0.25	r_1	0.4	r_2	0.6
s	0.8	d	2.5	a	0.9
cr	1.8	p_1	0.7	p_2	0.66
p_3	0.8				

the middle layer. The blind vias are drilled from Substrate 3 to Substrate 4. Fig. 2 shows the detailed geometry of each metal layer. To generate vertical polarization, four SIW H-plane horn antennas are constructed in Substrates 2, 3, and 4 between the middle layer and the bottom layer. The side boundaries of the SIW horn antennas are composed with the through vias. Two additional through vias are placed on the apertures of each horn antenna for V-pol bandwidth improvement. In order to reduce the distance between two adjacent horns, the apertures of each horn are overlapping. Each horn element is excited by a blind via, which is connected to a mini-SMP connector through a coplanar waveguide (CPW) on the bottom layer. This connecting structure is depicted in detail in Fig. 2(d). The H-pol radiation is generated by four dipole antennas on the top layer and the middle layer. Each dipole has one arm connected to the ground on the middle layer, and the other arm is connected to a microstrip line on the top layer. The microstrip lines have very thin and low profile so that the radiation loss is very low. The orientation of each dipole is inversed to its neighbor. The other end of the microstrip lines is connected to mini-SMP connectors using four through vias from the top layer to the bottom layer. Other through vias are placed around to suppress the radiation of these four vias. The footprint of the connecting structure is the same as that of the V-pol mode with the only difference that the CPW is omitted. The detailed dimensions are listed in Table I. All the vias used in the antenna share the same radius of 0.2 mm. The proposed antenna array has a small clearance of 1.8 mm and a low profile of 2.2 mm.

B. Operating Principles of the Antenna Element

To illustrate the operating principle of the proposed antenna array, the single antenna element is investigated here. As shown in Fig. 3, each antenna element contains an SIW horn and a dipole for vertical and horizontal polarizations. The connectors and their related structures are replaced with 50 Ω coaxial ports in this section. The simulated S-parameters are depicted in Fig. 4, demonstrating that the antenna element is able to cover the 5G bands of N257 (26.5–29.5 GHz) and N258 (24.25–27.5 GHz) in terms of impedance matching. In particular, the −10 dB impedance bandwidths are

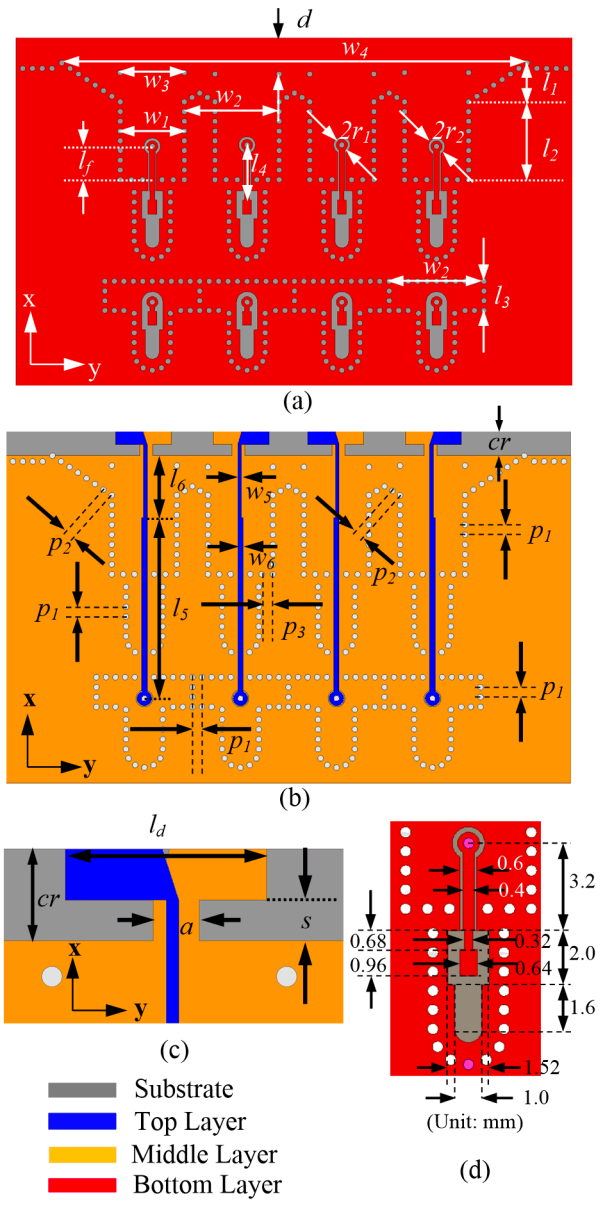

Fig. 2. Geometry of the proposed antenna array from (a) bottom view, (b) top view, (c) zoomed-in view of the dipole, and (d) zoomed-in view of the transitions between the blind via and the connector.

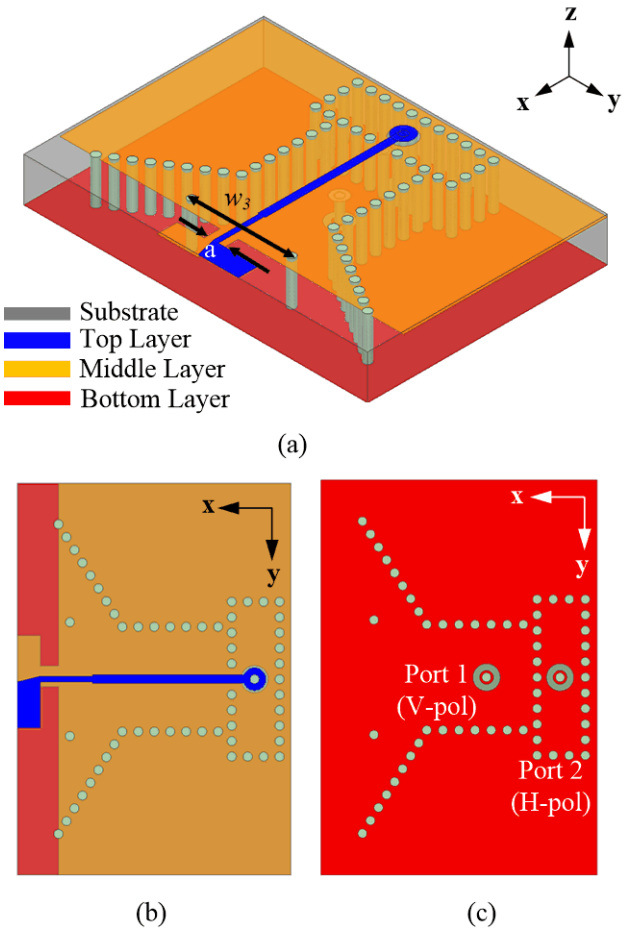

Fig. 3. Structure of the DP antenna element from (a) perspective view, (b) top view, and (c) bottom view.

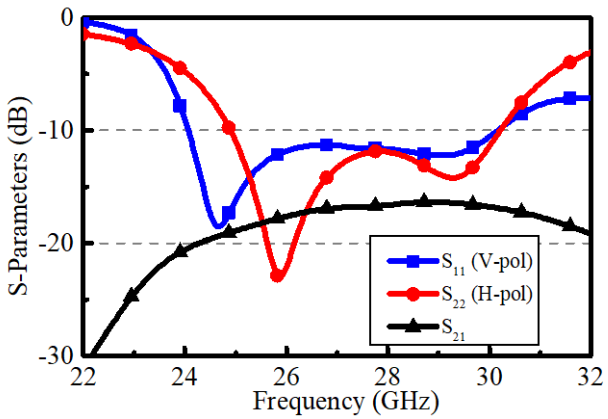

Fig. 4. Simulated S-parameters of the DP antenna element.

24.08–30.15 and 24.9–30.2 GHz for vertical and horizontal polarizations, respectively. The isolation between two ports is higher than 16.3 dB. Two matching vias are loaded at the horn aperture, which is proved to be a useful structure for improving the impedance matching of an SIW horn as reported in [33]. In this design, these vias are utilized for impedance bandwidth improvement of vertical polarization. To illustrate the working mechanism, a parametric analysis has been launched on the positions of these vias. In Fig. 5(a), the reflection coefficients are presented when the distance of the vias w_3 is 4.7, 5.0, and 5.3 mm, compared with the case without via loading. The unloaded antenna only has an impedance bandwidth of 3.5 GHz from 26.5 to 30 GHz. As w_3 increases, the impedance matching near 24 GHz is improved while that near 29.5 GHz almost remains the same. The input impedances of the V-pol mode with respect to w_3 are shown in the Smith chart as depicted in Fig. 5(b). To explain this phenomenon, we investigate the field distributions for the V-pol mode. Fig. 6 shows the magnitude of complex electric fields inside the SIW horn at different frequencies with and without vias. At 24.25 GHz, the TE_{10} mode is excited on the aperture for the unloaded case since the electric field

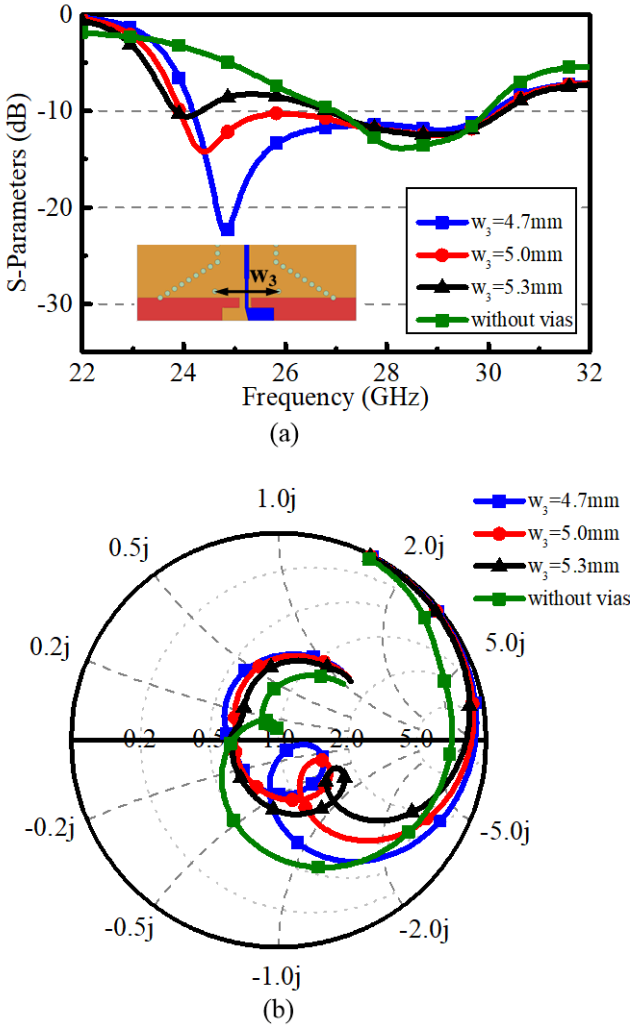

Fig. 5. Impedance properties of the vertical polarization port with respect to the distance of the vias. (a) Reflection coefficients. (b) Smith chart.

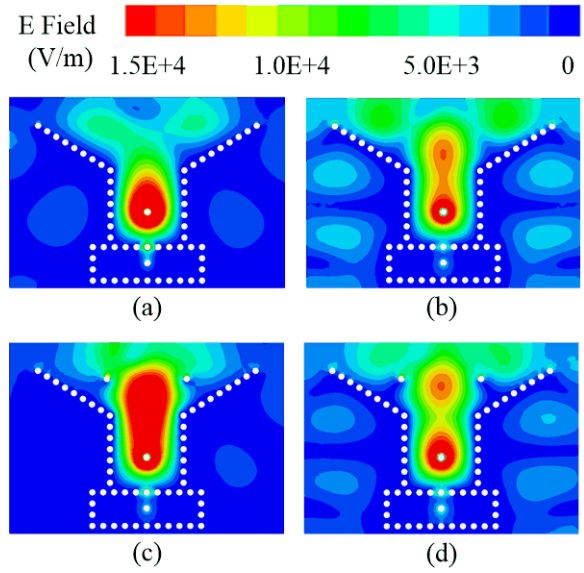

Fig. 6. Magnitude of the electric field distribution excited by the vertical polarization port at (a) 24.25 GHz without vias, (b) 29.5 GHz without vias, (c) 24.25 GHz with vias, and (d) 29.5 GHz with vias.

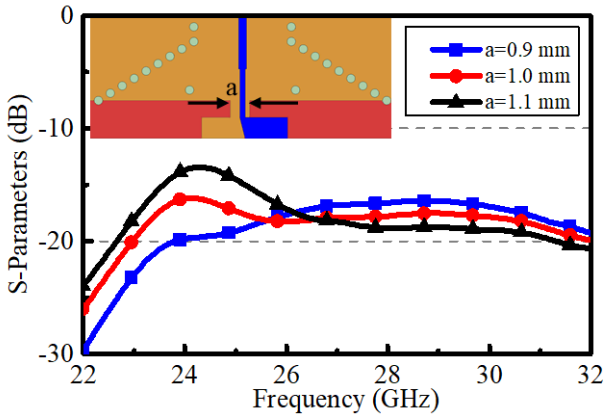

Fig. 7. Various mutual couplings between two polarizations with respect to different a.

presents a sinusoidal distribution. The width of the aperture is larger than half wavelength. Therefore, the input impedance is capacitive, which is corresponding to Fig. 5(b). As discussed in [33], the metal vias at the horn's aperture introduce an additional shunt inductance, which balances the conductance of the TE_{10} mode. At 29.5 GHz, the electric field distribution on the aperture is TE_{30} mode and two nulls can be observed near the loading place whether the vias exist or not. Therefore, the vias have little effects on the input impedance at 29.5 GHz. To obtain a wide bandwidth, w_3 is chosen to be 5.0 mm in the single antenna element, which is different from that in the antenna array, as shown in Table I. The isolation between the H-pol and V-pol modes is influenced by the width of the connecting stub, as shown in Fig. 7. An increasement of a leads to an isolation enhancement near 29 GHz but at the expense of mutual coupling deterioration near 24 GHz. A tradeoff optimization is considered for this parameter choose.

The element's normalized radiation patterns at 25 GHz of both polarizations are depicted in Fig. 8. For the vertical polarization, the simulated gain at endfire $(+x)$ direction is 4.0 dBi. The cross-polarization level is 5.7 dB lower than the co-polarization in the xy plane as shown in Fig. 8(b). For the H-pol mode, the endfire gain is 3.4 dBi. Different from the symmetrical radiation pattern of the V-pol mode, the radiation pattern of the H-pol mode in the xz plane is slightly up-tilted because of the extended ground plane below the dipole [33]. This issue is inevitable due to the demanding of a complete ground plane raised by 5G mmW antennas designed for handsets.

C. Four-Element Antenna Array Design

Based on the antenna element, a four-element array is built to achieve high gains and beam-scanning abilities. Since the size of the element is large, grating lobes will be generated when simply arranging four elements one by one. A solution to this problem is to overlap some part of the adjacent horn apertures. The distance between two adjacent elements is reduced to approximately half wavelength, as shown in Fig. 9. The four vertical polarization ports are numbered from Port

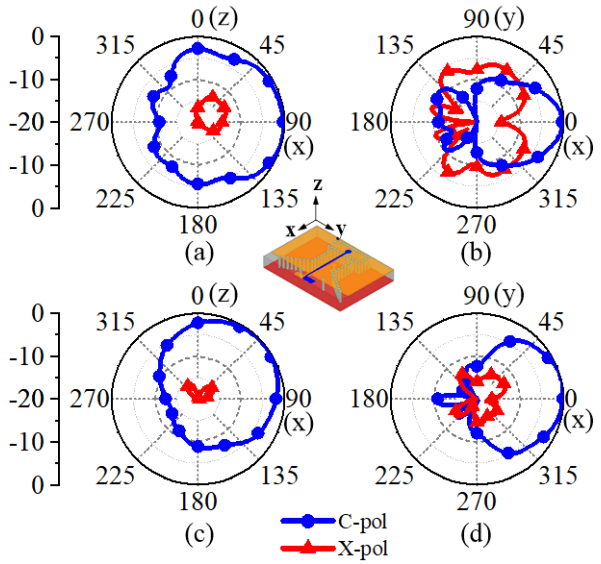

Fig. 8. Radiation patterns of the DP antenna element at 25 GHz in (a) *xz* plane and (b) *xy* plane for vertical polarization and (c) *xz* plane and (d) *xy* plane for horizontal polarization.

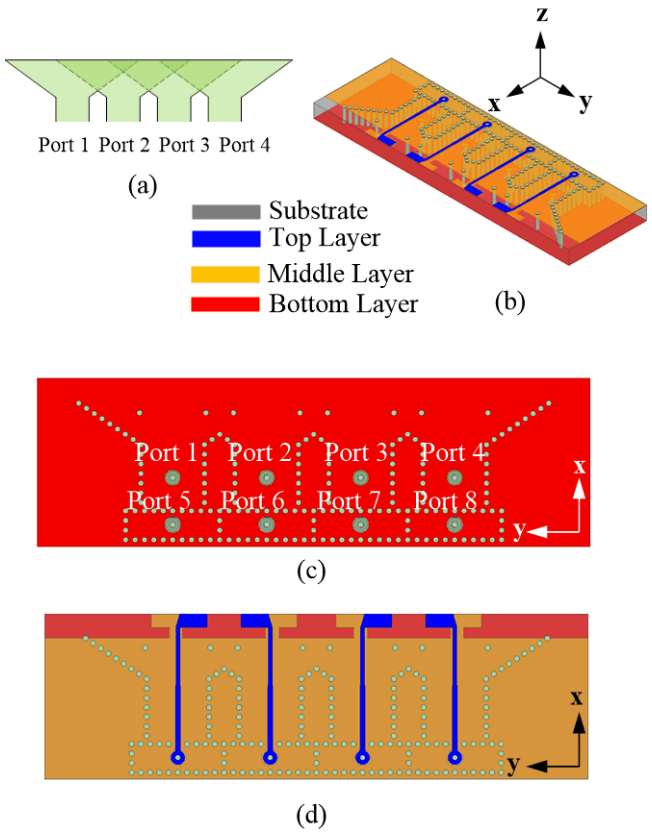

Fig. 9. Structure of the four-element antenna array with overlapped apertures. (a) Generalized geometry. (b) Perspective view. (c) Bottom view. (d) Top view.

1 to Port 4 and the four horizontal polarization ports are numbered from Port 5 to Port 8. Fig. 10 shows the magnitudes of the electric fields when Ports 1–4 are excited with different phase distributions. The electric field distributions of each port are similar to those depicted in Fig. 6 where one can

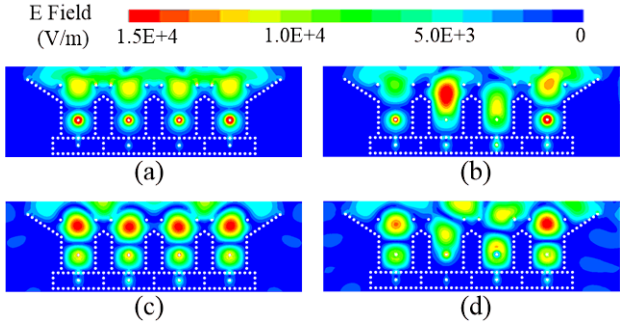

Fig. 10. Snapshots on the magnitudes of the electric fields when Ports 1–4 are excited at 24.25 GHz with a phase gradient of (a) 0° and (b) 120° and at 29.5 GHz with a phase gradient of (c) 0° and (d) 120°.

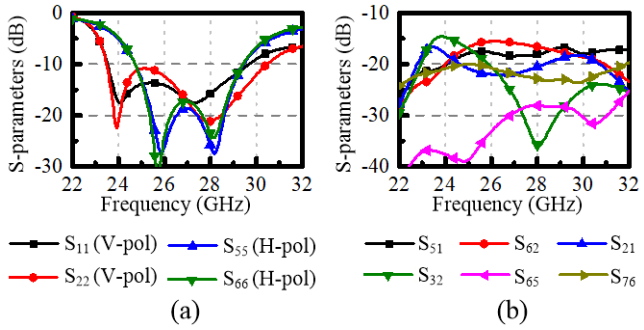

Fig. 11. Simulated S-parameters of the proposed DP antenna array. (a) Reflection coefficients. (b) Mutual couplings.

observe the TE_{10} modes at 24.25 GHz and the TE_{30} modes at 29.5 GHz. In this array, the TE_{30} modes are slightly distorted because the aperture is overlapping with the adjacent ones. When the ports are excited with a phase gradient of 120°, the wavefront is steered, indicating a beam-scanning ability. The simulated S-parameters are plotted in Fig. 11. In Fig. 11(a), the reflection coefficients of Ports 1, 2, 5, and 6 are shown for simplicity. The impedance bandwidths of the V-pol and H-pol modes are 23.37–29.60 and 24.87–29.66 GHz, respectively. The isolations are illustrated in Fig. 11(b) to show the mutual couplings between adjacent ports. The isolations are higher than 15 dB within the operating bands. In order to describe the impedance properties of the phased array more sufficiently, the active S-parameters are also simulated and depicted in Fig. 12 under different excitation conditions: Ports 1–4, Ports 5–8, and Ports 1–8. The active S-parameters of some ports are aggregated to no more than −9 dB in some extreme conditions. Nevertheless, the active S-parameters are similar to the passive ones in most conditions because of the high isolations among the ports, demonstrating good impedance matching when the beam is steered.

To perform a better cross-polarization suppression for the horizontal polarization, two different array arrangements of the dipole elements have been investigated and a comparison has been made. To achieve an endfire radiation to the $+x$-direction, the used array is fed out-of-phase with 180° interval as used in [34], shown in Fig. 13(a), while the reference array is with in-phase feed, as shown in Fig. 13(b). Fig. 13(c) and (d)

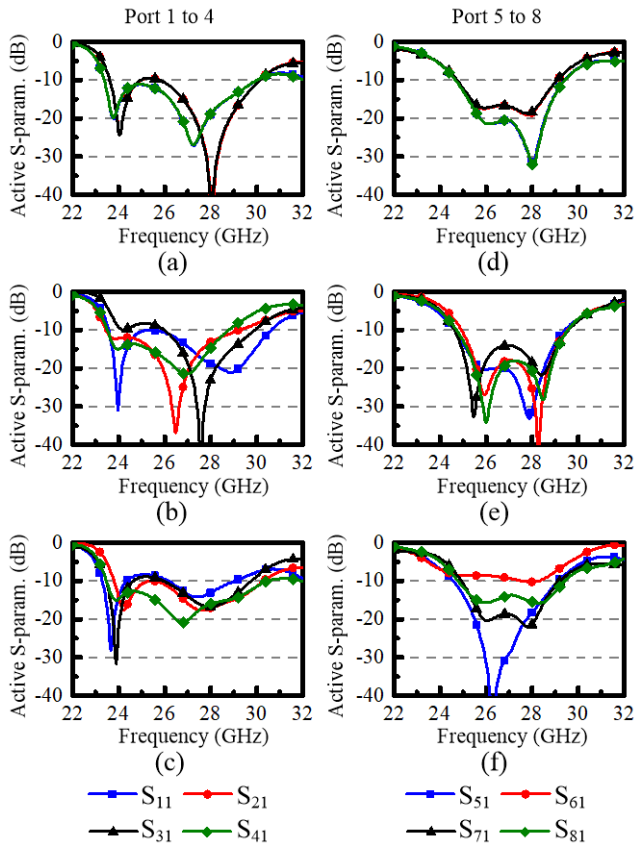

Fig. 12. Simulated active S-parameters of the eight ports of the proposed DP antenna array: active S-parameters of Ports 1–4 under the phase gradient of (a) 0° and (b) 120° when only Ports 1–4 are excited and (c) when Ports 1–8 are excited with a phase distribution of (0°, 0°, 0°, 0°, 0°, 180°, 0°, 180°). (d)–(f) Active S-parameters of Ports 5–8 under phase distributions of (0°, 180°, 0°, 180°), (0°, 60°, 120°, 180°), and (0°, 0°, 0°, 0°, 0°, 180°, 0°, 180°).

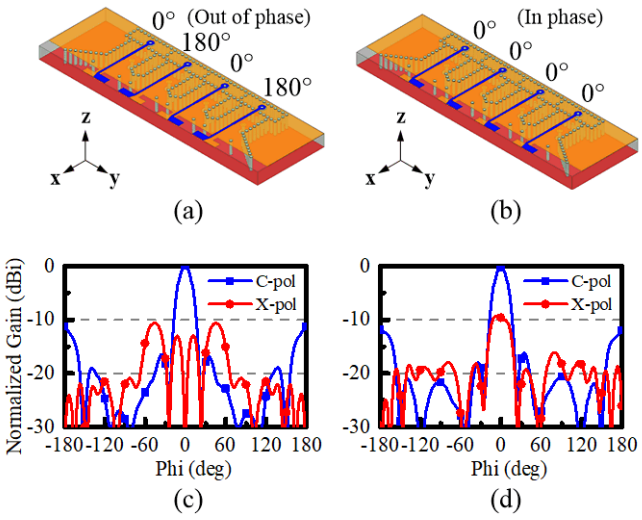

Fig. 13. Comparison between two different dipole arrangements: array structures in which the adjacent elements are (a) out-of-phase or (b) in-phase and normalized patterns of (c) out-of-phase and (d) in-phase array.

plot the normalized radiation pattern of two cases with cross polarizations. It is shown that the proposed out-of-phase design is beneficial for cross polarization suppression at the $+x$-direction.

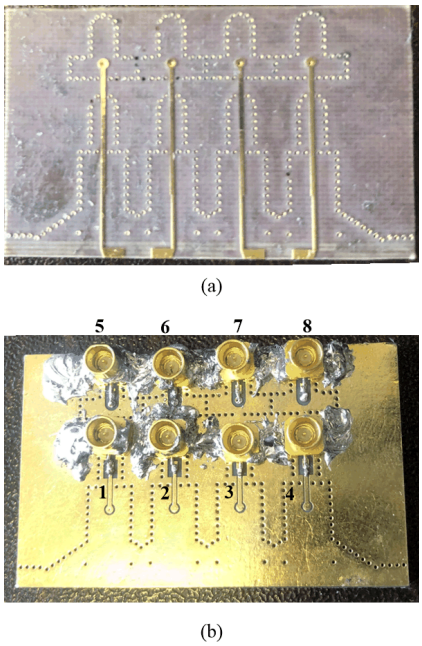

Fig. 14. Fabricated antenna prototype from (a) top view and (b) bottom view.

III. Antenna Fabrication and Measurements

To validate the proposed design, a prototype is constructed and measured. The antenna is fabricated using multilayer PCB technique and a photograph of the prototype is shown in Fig. 14. The eight ports are numbered from 1 to 8 as depicted in Fig. 14(b). The reflection coefficients and mutual couplings of all the eight ports are measured using a vector network analyzer. In Fig. 15, the measured S-parameters of the antennas are shown and compared with the simulated data. Fig. 15(a) shows the reflection coefficients of Port 1 and Port 2. The measured impedance bandwidth of the V-pol modes in which the reflection coefficients are smaller than -10 dB is 29.1% from 23.2 to 31.1 GHz, while the simulated one is 29.2% from 23.6 to 31.7 GHz. The mutual couplings between either two ports among Ports 1, 2, 3, and 4 are measured to be lower than -15 dB, demonstrating high port isolation between horn elements. The measured S-parameters agree well with the simulated ones. The S-parameters of the H-pol modes (Ports 5–8) are measured and depicted in Fig. 15(c) and (d). The measured and simulated impedance bandwidths are 20.5% from 24.0 to 29.5 GHz and 19.0% from 24.4 to 29.5 GHz, respectively. The simulated and measured isolations are higher than 20 dB. The measured results validate acceptable performance on impedance bandwidth and isolation.

The radiation properties of the proposed antenna array are measured in an anechoic chamber. In Fig. 16, the patterns in the *xy* plane and *xz* plane excited by Ports 1, 2, 5, and 6 at 25 and 29 GHz are listed. Slight distortions are observed in the radiation patterns excited by Ports 1 and 2. The distortions in the *xy* plane are mainly caused by the difference between the boundary conditions of a single antenna element and that in the antenna array. The distortions in the *xz* plane are mainly caused by the scatterings of backward radiations by

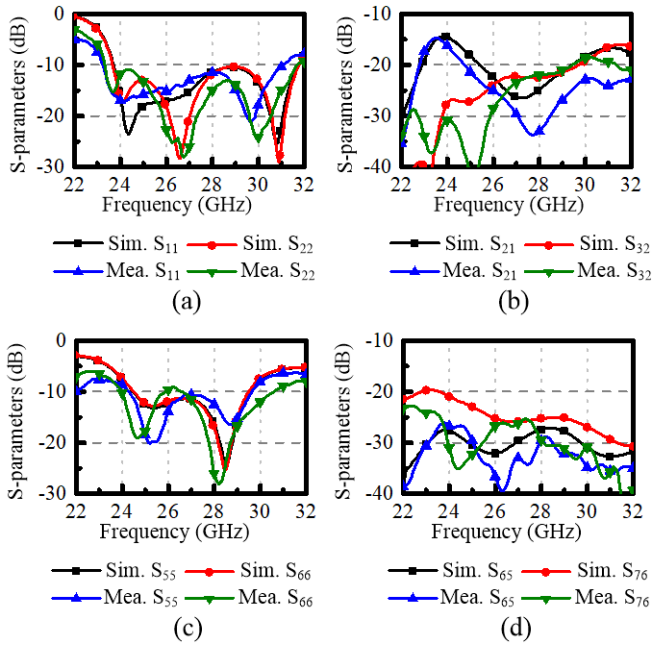

Fig. 15. Simulated and measured S-parameters of the antenna. (a) Reflection coefficients and (b) mutual couplings of the V-pol ports (Ports 1–4). (c) Reflection coefficients and (d) mutual couplings of the H-pol ports (Ports 5–8).

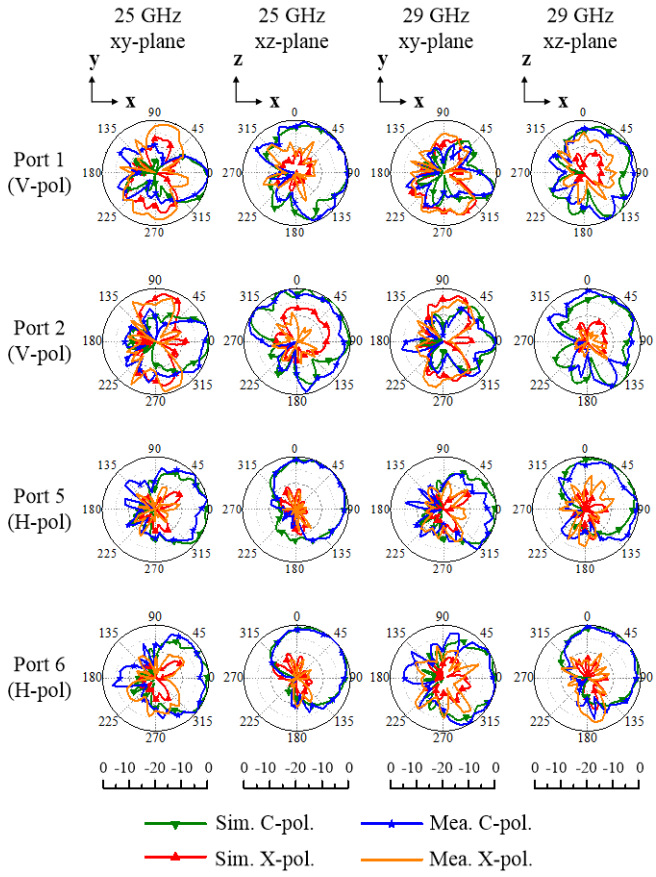

Fig. 16. Simulated and measured radiation patterns in the *xy* plane and *xz* plane at 25 and 29 GHz excited by Ports 1, 2, 5, and 6.

the connectors beneath the ground planes. For the H-pol case, the distortions are not obvious because the backward radiation is low.

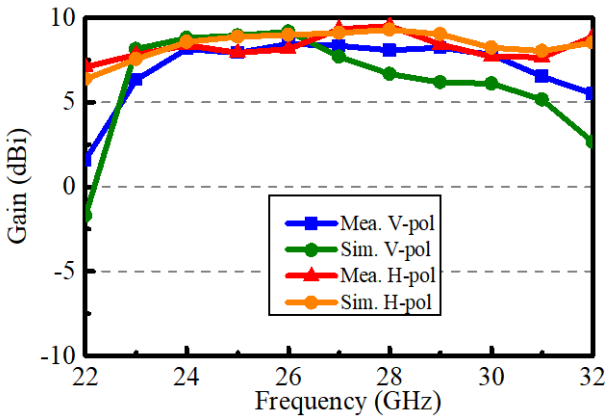

Fig. 17. Simulated and measured gains of the antenna when the beam is steered at the *x*-direction of the H-pol mode and V-pol mode.

TABLE II
COMPARISON AMONG THE PROPOSED DESIGN AND OTHER DP ENDFIRE mmW ANTENNA ARRAYS

Ref.	Element number	BW (%)	Thickness (λ_0)	Clearance (λ_0)	3dB scanning range
[29]	1×4	26.3	0.23	Not given	Not given
[31]	1×4	22.5	0.37	0.35	±38°
[32]	1×4	7.0	0.1	0.25	-42° to 39° (above 4 dBi)
This work	**1×4**	**19.0**	**0.19**	**0.16**	**-34° to 33°**

Based on the measured radiation patterns excited by all the eight ports, we synthesize the total radiation patterns of the whole antenna array when the ports are fed with different phases. Fig. 17 shows a comparison between the simulated gains and the calculated gains of the antenna array based on the measured results of both polarizations. For the V-pol case, the antenna array's gain at endfire direction reaches its maximum when Ports 1–4 are excited with the same phase and magnitude. A 180° phase gradient is adopted for the horizontal polarization when the beam is steered at the endfire direction. The calculated results based on the measured data match well with the simulated ones. The beam-scanning performances have also been calculated based on the measured radiation patterns of each element. The 3 dB beam-scanning range from −34° to 33° is covered by both the V-pol and H-pol modes. In particular, the 3 dB beam-scanning range is from −34° to 33° for vertical polarization, while −39° to 40° for horizontal case. The radiation patterns for these cases are shown in Fig. 18. The scanning range of the H-pol mode is larger than that of the V-pol one because the element's beamwidth of the H-pol mode is wider than that of the V-pol one. In addition, higher mutual couplings between adjacent ports of the V-pol modes also limit the scanning abilities of the V-pol modes.

To further validate the advantages of the proposed design, a comparison is performed with other mmW endfire antennas [29], [31], [32]. In Table II, the performances of different designs are listed and compared. Among them, the proposed

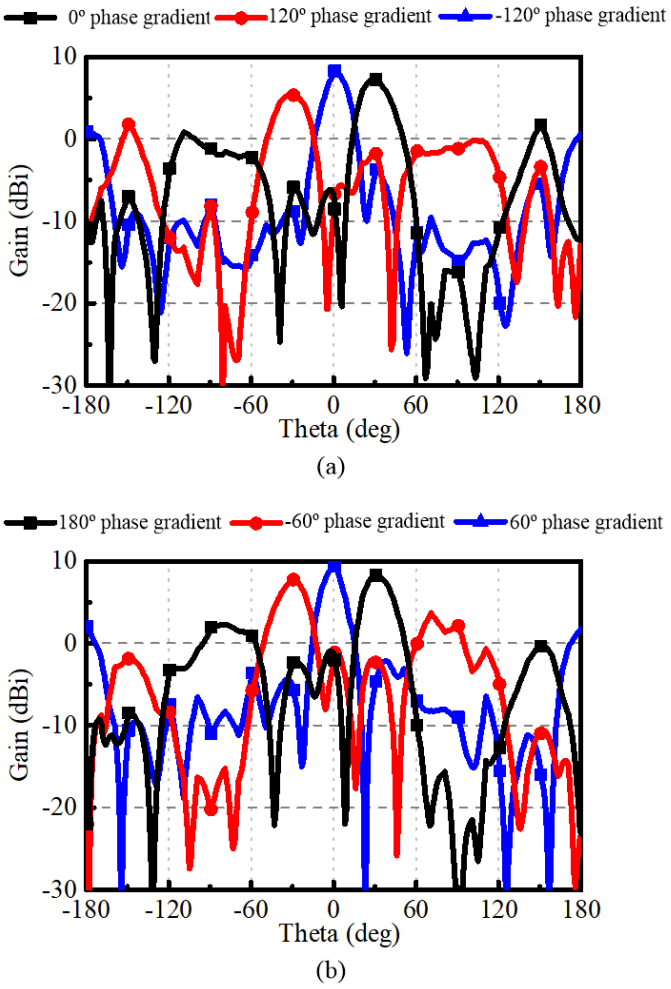

Fig. 18. Beam-scanning properties of the proposed antenna array: radiation patterns at 27 GHz in the *xy* plane of (a) V-pol and (b) H-pol modes excited by different phase distributions.

antenna array is with merits of small clearance and low profile, making it more suitable for space-limited applications. The thickness of profile is related to the bandwidth but limited by the device volume. In particular, the bandwidth of the V-pol mode, which is measured to be 29.1%, is competitive against other linear polarized works. Instead of loading dielectrics or metasurfaces, the via-loading method effectively reduces the ground clearance. Compared with [32], the proposed antenna array can cover the 5G mmW band from 24.25 to 27.5 GHz within a smaller clearance and wider impedance bandwidth. In addition, the beam-scanning performances are also compared. Compared with [31], the scanning range of the proposed design is a bit limited. This is due to the narrow beamwidth of each element and the large intercept between the elements, which are inevitable when the element's size is large enough for a wideband performance and good isolations.

IV. Conclusion

In this article, a DP antenna array with endfire radiation pattern has been designed within a profile of 2.2 mm and a small clearance of 1.8 mm. By combining the SIW horn antennas and the dipole antennas, both the V-pol and H-pol modes are excited through different ports. Two vias are loaded on the aperture of each horn element for bandwidth enhancement of the V-pol modes without extra clearance used. In addition, an overlapped-aperture method is adopted to reduce the distance between two adjacent antenna elements when composing the four-element antenna array. This antenna array has been proved by both the simulations and measurements, including a bandwidth of 19.0%, a maximum gain of 9.16 dBi, and a 3 dB scanning range from −34° to 33°. The proposed design presents an ability of covering two valuable bands of 24.25–27.5 and 26.5–29.5 GHz, making it suitable for 5G wireless communications at mmW bands on handsets or AiP applications.

References

[1] T. S. Rappaport *et al.*, "Millimeter wave mobile communications for 5G cellular: It will work!" *IEEE Access*, vol. 1, pp. 335–349, May 2013.

[2] W. Hong, K.-H. Baek, and S. Ko, "Millimeter-wave 5G antennas for smartphones: Overview and experimental demonstration," *IEEE Trans. Antennas Propag.*, vol. 65, no. 12, pp. 6250–6261, Dec. 2017.

[3] W. Roh *et al.*, "Millimeter-wave beamforming as an enabling technology for 5G cellular communications: Theoretical feasibility and prototype results," *IEEE Commun. Mag.*, vol. 52, no. 2, pp. 106–113, Feb. 2014.

[4] L. Chang, Y. Li, Z. Zhang, X. Li, S. Wang, and Z. Feng, "Low-sidelobe air-filled slot array fabricated using silicon micromachining technology for millimeter-wave application," *IEEE Trans. Antennas Propag.*, vol. 65, no. 8, pp. 4067–4074, Aug. 2017.

[5] N. Ojaroudiparchin, M. Shen, S. Zhang, and G. F. Pedersen, "A switchable 3-D-coverage-phased array antenna package for 5G mobile terminals," *IEEE Antennas Wireless Propag. Lett.*, vol. 15, pp. 1747–1750, 2016.

[6] A. A. Baba, R. M. Hashmi, K. P. Esselle, J. G. Marin, and J. Hesselbarth, "Broadband partially reflecting superstrate-based antenna for 60 GHz applications," *IEEE Trans. Antennas Propag.*, vol. 67, no. 7, pp. 4854–4859, Jul. 2019.

[7] M. Ettorre, E. Gandini, and R. Sauleau, "Multi-beam pillbox antennas in the millimeter-wave range," in *Proc. 5th Eur. Conf. Antennas Propag. (EUCAP)*, Rome, Italy, 2011, pp. 2947–2950.

[8] D. G. Lopez and D. S. Filipovic, "On the design of milimeter-wave antennas for amplitude-only direction finding," in *Proc. IEEE Int. Symp. Phased Array Syst. Technol. (PAST)*, Waltham, MA, USA, Oct. 2016, pp. 1–8.

[9] E. Arnieri, L. Boccia, and G. Amendola, "A ka-band dual-frequency radiator for array applications," *IEEE Antennas Wireless Propag. Lett.*, vol. 8, pp. 894–897, 2009.

[10] R. Gomes, J. Reis, Z. Al-Daher, A. Hammoudeh, and R. F. S. Caldeirinha, "5G: Performance and evaluation of FS-FBMC against OFDM for high data rate applications at 60 GHz," *IET Signal Process.*, vol. 12, no. 5, pp. 620–628, Jul. 2018.

[11] E. Al Abbas, N. Nguyen-Trong, A. T. Mobashsher, and A. M. Abbosh, "Polarization-reconfigurable antenna array for millimeter-wave 5G," *IEEE Access*, vol. 7, pp. 131214–131220, 2019.

[12] R. J. Bolt *et al.*, "Characterization of a dual-polarized connected-dipole array for ku-band mobile terminals," *IEEE Trans. Antennas Propag.*, vol. 64, no. 2, pp. 591–598, Feb. 2016.

[13] Q. Yang *et al.*, "Dual-polarized crossed slot array antenna designed on a single laminate for millimeter-wave applications," *IEEE Trans. Antennas Propag.*, vol. 68, no. 5, pp. 4120–4125, May 2020.

[14] Y. Li and K.-M. Luk, "60-GHz dual-polarized two-dimensional switch-beam wideband antenna array of aperture-coupled magneto-electric dipoles," *IEEE Trans. Antennas Propag.*, vol. 64, no. 2, pp. 554–563, Feb. 2016.

[15] S. Liao and Q. Xue, "Dual polarized planar aperture antenna on LTCC for 60-GHz antenna-in-package applications," *IEEE Trans. Antennas Propag.*, vol. 65, no. 1, pp. 63–70, Jan. 2017.

[16] G.-N. Tan, X.-X. Yang, and B. Han, "A dual-polarized Fabry–Pérot cavity antenna at millimeter wave band with high gain," in *Proc. IEEE 4th Asia–Pacific Conf. Antennas Propag. (APCAP)*, Kuta, Indonesia, Jun. 2015, pp. 621–622.
[17] Z. Ahmad and J. Hesselbarth, "On-chip dual-polarized dielectric resonator antenna for millimeter-wave applications," *IEEE Antennas Wireless Propag. Lett.*, vol. 17, no. 10, pp. 1769–1772, Oct. 2018.
[18] S. Lee, S. Kim, and J. Choi, "Dual-band dual-polarized proximity fed patch antenna for 28 GHz/39 GHz 5G millimeter-wave communications," in *Proc. 13th Eur. Conf. Antennas Propag. (EuCAP)*, Krakow, Poland, 2019, pp. 1–5.
[19] C. Di Paola, S. Zhang, K. Zhao, Z. Ying, T. Bolin, and G. F. Pedersen, "Wideband beam-switchable 28 GHz quasi–Yagi array for mobile devices," *IEEE Trans. Antennas Propag.*, vol. 67, no. 11, pp. 6870–6882, Nov. 2019.
[20] A. Dadgarpour, B. Zarghooni, B. S. Virdee, and T. A. Denidni, "Millimeter-wave high-gain SIW end-fire bow-tie antenna," *IEEE Trans. Antennas Propag.*, vol. 63, no. 5, pp. 2337–2342, May 2015.
[21] Y. Zhang, Z. Xue, and W. Hong, "Planar substrate-integrated endfire antenna with wide beamwidth for Q-band applications," *IEEE Antennas Wireless Propag. Lett.*, vol. 16, pp. 1990–1993, 2017.
[22] Y. Cai *et al.*, "Compact wideband SIW horn antenna fed by elevated-CPW structure," *IEEE Trans. Antennas Propag.*, vol. 63, no. 10, pp. 4551–4557, Oct. 2015.
[23] Y. Cai, Z.-P. Qian, Y.-S. Zhang, J. Jin, and W.-Q. Cao, "Bandwidth enhancement of SIW horn antenna loaded with air-via perforated dielectric slab," *IEEE Antennas Wireless Propag. Lett.*, vol. 13, pp. 571–574, 2014.
[24] M. Esquius-Morote, B. Fuchs, J.-F. Zurcher, and J. R. Mosig, "A printed transition for matching improvement of SIW horn antennas," *IEEE Trans. Antennas Propag.*, vol. 61, no. 4, pp. 1923–1930, Apr. 2013.
[25] M. Esquius-Morote, B. Fuchs, J.-F. Zurcher, and J. R. Mosig, "Novel thin and compact H-plane SIW horn antenna," *IEEE Trans. Antennas Propag.*, vol. 61, no. 6, pp. 2911–2920, Jun. 2013.
[26] N. Bayat-Makou, M. S. Sorkherizi, and A. A. Kishk, "Substrate integrated horn antenna loaded with open parallel transitions," *IEEE Antennas Wireless Propag. Lett.*, vol. 16, pp. 349–351, 2017.
[27] T. Li and Z. N. Chen, "Wideband substrate-integrated waveguide-fed endfire metasurface antenna array," *IEEE Trans. Antennas Propag.*, vol. 66, no. 12, pp. 7032–7040, Dec. 2018.
[28] W. Hong, S.-T. Ko, Y. Lee, and K.-H. Baek, "Multi-polarized antenna array configuration for mmWave 5G mobile terminals," in *Proc. Int. Workshop Antenna Technol. (iWAT)*, Seoul, South Korea, Mar. 2015, pp. 60–61.
[29] Y.-W. Hsu, T.-C. Huang, H.-S. Lin, and Y.-C. Lin, "Dual-polarized quasi Yagi–Uda antennas with endfire radiation for millimeter-wave MIMO terminals," *IEEE Trans. Antennas Propag.*, vol. 65, no. 12, pp. 6282–6289, Dec. 2017.
[30] A. Li and K.-M. Luk, "Millimeter-wave dual linearly polarized endfire antenna fed by 180° hybrid coupler," *IEEE Antennas Wireless Propag. Lett.*, vol. 18, no. 7, pp. 1390–1394, Jul. 2019.
[31] Q. Wu, J. Hirokawa, J. Yin, C. Yu, H. Wang, and W. Hong, "Millimeter-wave multibeam endfire dual-circularly polarized antenna array for 5G wireless applications," *IEEE Trans. Antennas Propag.*, vol. 66, no. 9, pp. 4930–4935, Sep. 2018.
[32] J. Zhang, K. Zhao, L. Wang, S. Zhang, and G. F. Pedersen, "Dual-polarized phased array with end-fire radiation for 5G handset applications," *IEEE Trans. Antennas Propag.*, vol. 68, no. 4, pp. 3277–3282, Apr. 2020.
[33] D. Sun, J. Xu, and S. Jiang, "SIW horn antenna built on thin substrate with improved impedance matching," *Electron. Lett.*, vol. 51, no. 16, pp. 1233–1235, Aug. 2015.
[34] Y. Zhao, Z. Shen, and W. Wu, "Effects of grounding platform on the radiation performance of H-plane horn antennas," in *Proc. IEEE Int. Conf. Microw. Millim. Wave Technol. (ICMMT)*, Beijing, China, Jun. 2016, pp. 656–658.
[35] L. Chang, Z. Zhang, Y. Li, and M. F. Iskander, "Single-layer magnetic current antenna array with high realized aperture usage rate based on microstrip line structure," *IEEE Trans. Antennas Propag.*, vol. 65, no. 2, pp. 584–592, Feb. 2017.

Hao Li received the B.S. degree in electronic engineering from Tsinghua University, Beijing, China, in 2018, where he is currently pursuing the Ph.D. degree in electronic engineering.

His current research interests include wideband antennas, millimeter-wave antenna arrays, metamaterials, and metamaterial-inspired antennas.

Mr. Li serves as a Reviewer for the IEEE TRANSACTIONS ON ANTENNAS AND PROPAGATION and *Microwave and Optical Technology Letters*.

Yue Li (Senior Member, IEEE) received the B.S. degree in telecommunication engineering from Zhejiang University, Hangzhou, China, in 2007 and the Ph.D. degree in electronic engineering from Tsinghua University, Beijing, China, in 2012.

In June 2012, he joined the Department of Electronic Engineering, Tsinghua University, as a Post-Doctoral Fellow. In December 2013, he joined the Department of Electrical and Systems Engineering, University of Pennsylvania, Philadelphia, PA, USA, as a Research Scholar. He was a Visiting Scholar with the Institute for Infocomm Research (I2R), A∗STAR, Singapore, in 2010 and the Hawaii Center of Advanced Communication (HCAC), University of Hawai'i at Mānoa, Honolulu, HI, USA, in 2012. Since January 2016, he has been with Tsinghua University, where he is currently an Assistant Professor and also an Associate Professor with the Department of Electronic Engineering. He has authored or co-authored over 140 journal articles and 45 international conference papers, and holds 18 granted Chinese patents. His current research interests include metamaterials, plasmonics, electromagnetics, nanocircuits, mobile and handset antennas, MIMO and diversity antennas, and millimeter-wave antennas and arrays.

Dr. Li was a recipient of the Issac Koga Gold Medal from URSI General Assembly in 2017, the Second Prize of the Science and Technology Award of the China Institute of Communications in 2017, the young scientist awards from the conferences of ACES 2018, AT-RASC 2018, AP-RASC 2016, EMTS 2016, and URSI GASS 2014, the best paper awards from the conferences of CSQRWC 2018, NCMMW 2018 and 2017, APCAP 2017, NCANT 2017, ISAPE 2016, and ICMMT 2016, the Outstanding Doctoral Dissertation of Beijing Municipality in 2013, and the Principal Scholarship of Tsinghua University in 2011. He is serving as an Associate Editor for the IEEE TRANSACTIONS ON ANTENNAS AND PROPAGATION, the IEEE ANTENNAS AND WIRELESS PROPAGATION LETTERS, *Microwave and Optical Technology Letters*, and *Computer Applications in Engineering Education*, and the Editorial Board of Scientific Report.

Le Chang received the B.S. degree in electronics and information engineering from Xidian University, Xi'an, China, in 2012 and the Ph.D. degree from Tsinghua University, Beijing, China, in 2017.

He is currently working as a Senior Engineer with the Consumer Business Group of Huawei Inc., Beijing.

Wangyu Sun (Graduate Student Member, IEEE) received the B.S. and M.S. degrees from Tsinghua University, Beijing, China, in 2016 and 2019, respectively, where he is currently pursuing the Ph.D. degree.

His current research interests include broadband antennas, low-profile antennas, and waveguide metatronics.

Xu Qin received the B.S. degree in electrical engineering from Tsinghua University, Beijing, China, in 2019, where he is currently pursuing the Ph.D. degree.

His research interests include metamaterials, small antenna, and microstrip antenna.

Hanyang Wang (Senior Member, IEEE) received the Ph.D. degree from Heriot-Watt University, Edinburgh, U.K., in 1995.

From 1986 to 1991, he served as a Lecturer and an Associate Professor with Shandong University, Jinan, China. From 1995 to 1999, he was a Post-Doctoral Research Fellow with the University of Birmingham, Birmingham, U.K., and the University of Essex, Colchester, U.K. From 1999 to 2000, he was a Software Development and Microwave and Antenna Engineering Consultant Engineer with Vector Fields Ltd., Oxford, U.K. He joined Nokia U.K. Ltd., Farnborough, U.K., in 2001, where he had been a Mobile Antenna Specialist for 11 years. Then, he joined the Consumer Business Group of Huawei Inc., Reading, U.K., where he is currently the Chief Mobile Antenna Expert and the Head of the Mobile Antenna Technology Division. He is also an Adjunct Professor with Nanjing University, Nanjing, China, and Sichuan University, Chengdu, China. His current research interests include small, wideband, and multiband antennas for mobile terminals, antennas, and antenna arrays for 5G mobile communications in sub-6 GHz and millimeter-wave (mm-wave) frequency bands. He has authored over 100 articles on these topics. He holds over 40 granted U.S./European/Japanese/Chinese patents.

Dr. Wang is a Huawei Fellow and an IET Fellow. He was a recipient of the Title of Nokia Inventor of the Year in 2005, the Nokia Excellence Award in 2011, the Huawei Individual Gold Medal Award in 2012, and the Huawei Team Gold Medal Award in 2013 and 2014. His patent was ranked number one among 2015 Huawei top ten patent awards. He is an Associate Editor of the IEEE ANTENNAS AND WIRELESS PROPAGATION LETTERS.